© 2022. Published by The Company of Biologists Ltd | Biology Open (2022) 11, bio058941. doi:10.1242/bio.058941

RESEARCH ARTICLE

Autism-associated CHD8 keeps proliferation of human neural progenitors in check by lengthening the G1 phase of the cell cycle

Emma Coakley-Youngs[1], Medhavi Ranatunga[2], Simon Richardson[3], Giulia Getti[2], Susan Shorter[1,‡] and Marc Fivaz[1,*,‡]

ABSTRACT

De novo mutations (DNMs) in chromodomain helicase DNA binding protein 8 (CHD8) are associated with a specific subtype of autism characterized by enlarged heads and distinct cranial features. The vast majority of these DNMs are heterozygous loss-of-function mutations with high penetrance for autism. CHD8 is a chromatin remodeler that preferentially regulates expression of genes implicated in early development of the cerebral cortex. How *CHD8* haploinsufficiency alters the normal developmental trajectory of the brain is poorly understood and debated. Using long-term single-cell imaging, we show that disruption of a single copy of *CHD8* in human neural precursor cells (NPCs) markedly shortens the G1 phase of the cell cycle. Consistent with faster progression of *CHD8*$^{+/-}$ NPCs through G1 and the G1/S checkpoint, we observed increased expression of E cyclins and elevated phosphorylation of Erk in these mutant cells – two central signaling pathways involved in S phase entry. Thus, *CHD8* keeps proliferation of NPCs in check by lengthening G1, and mono-allelic disruption of this gene alters cell-cycle timing in a way that favors self-renewing over neurogenic cell divisions. Our findings further predict enlargement of the neural progenitor pool in *CHD8*$^{+/-}$ developing brains, providing a mechanistic basis for macrocephaly in this autism subtype.

KEY WORDS: Autism, ASD, Stem cell, Cortical development, Chromatin, CRISPR/Cas gene editing, CHD8, Cell cycle

INTRODUCTION

Recent exome sequencing studies from family trios have led to the identification of numerous spontaneous mutations associated with autism spectrum disorder (ASD) (Bernier et al., 2014; Barnard et al., 2015; O'Roak et al., 2012; Weiss et al., 2016; Helsmoortel et al., 2014; An et al., 2020). Among these, *de novo* mutations (DNMs) in the ATP-dependent chromatin remodeler chromodomain helicase DNA binding protein 8 (CHD8) have attracted considerable attention. CHD8 is one of the most frequently mutated genes in ASD – 20 different DNMs have so far been identified, most of which are predicted loss-of-function (LoF) mutations on a single gene copy with high penetrance for ASD (Barnard et al., 2015; An et al., 2020). *CHD8* DNMs give rise to a distinct ASD subtype characterized by enlarged head circumference, dysmorphic facial features and gastrointestinal problems. Notably, macrocephaly is observed in 15% of autistic individuals (Fombonne et al., 1999; Fidler et al., 2000), but the exact nature of this association and the mechanisms underlying macrocephaly in ASD (including the CHD8 ASD subtype), are subject to debate (Fidler et al., 2000; Gompers et al., 2017; Durak et al., 2016).

Chromodomain helicase DNA-binding proteins belong to one of four subfamilies of chromatin remodelers (Hota and Bruneau, 2016) that use energy from ATP to slide along DNA – a process involved in nucleosome repositioning (Lai and Pugh, 2017). CHD8 expression in the brain peaks during mid-gestational life and is particularly elevated in cortical progenitors and post-mitotic neocortical layers (Bernier et al., 2014), pointing to early corticogenesis as a likely target of *CHD8* DNMs. Accordingly, this chromatin remodeler preferentially influences the expression of genes implicated in neocortical development (Gompers et al., 2017; Suetterlin et al., 2018; Wang et al., 2017), including other ASD risk factors (Sugathan et al., 2014; Cotney et al., 2015). RNA-seq studies in various models of *CHD8* haploinsufficiency identified several gene modules regulated by CHD8: RNA processing, cell cycle regulation, neuronal development and differentiation, and synapse function (Gompers et al., 2017; Suetterlin et al., 2018; Wang et al., 2017; Sugathan et al., 2014; Platt et al., 2017; Jung et al., 2018; Katayama et al., 2016), but a clear picture of the role of this chromatin remodeler in brain development is yet to emerge.

While macrocephaly is observed in several independent mouse models of *CHD8* haploinsufficiency (Gompers et al., 2017; Suetterlin et al., 2018; Platt et al., 2017), surprisingly little is known about the function of this gene in cortical assembly. In an early study, silencing of *CHD8* in mouse embryos by RNA interference resulted in reduced proliferation of NPCs and accelerated neuronal differentiation (Durak et al., 2016), an effect attributed to decreased transcription of genes regulating the cell cycle and Wnt signaling. This finding is in line with other reports in non-neuronal tissues describing a stimulatory effect of CHD8 on cell proliferation (Subtil-Rodríguez et al., 2014; Menon et al., 2010) via E2F-dependent transcriptional activation of S phase genes (Subtil-Rodríguez et al., 2014; Rodríguez-Paredes et al., 2009). In marked contrast, germline haploinsufficiency of *CHD8* in mice is associated with a ∼20% global increase in proliferation of cortical progenitors, and a specific increase in the number of Pax6^{+} radial glial cells located in the subventricular zone of the developing cortex (Gompers et al., 2017). This view is aligned with another recent report describing an inhibitory function of *kismet*, the fly

[1]Stem Cell & Gene Editing Laboratory, University of Greenwich at Medway, Faculty of Science and Engineering, Kent ME4 4TB, UK. [2]University of Greenwich at Medway, Faculty of Science and Engineering, Kent ME4 4TB, UK. [3]Exogenics Laboratory, University of Greenwich at Medway, Faculty of Science and Engineering, Kent ME4 4TB, UK.
*Present address: reMYND, Bio-Incubator, Gaston Geeslaan 1, 3001 Leuven-Heverlee, Belgium.

‡Authors for correspondence (susan.shorter@greenwich.ac.uk; marc.fivaz@remynd.com).

S.R., 0000-0002-7927-0649; G.G., 0000-0003-1402-8496; M.F., 0000-0003-1003-7934

Received 23 July 2021; Accepted 28 July 2022

Biology Open (2022) 11, bio058941. doi:10.1242/bio.058941

analog of *CHD8*, in intestinal stem cell proliferation (Gervais et al., 2019), and an increasing number of studies implicating *CHD8* as a tumor suppressor (Sawada et al., 2013). While context-dependent functions of CHD8 could account for opposing outcomes in different species and cell types (Durak et al., 2016; Rodríguez-Paredes et al., 2009), the cause of these conflicting reports in mouse developing cortex is unclear, and is likely to be multifactorial (gene dosage, timing of *CHD8* knockdown by RNAi, cell-autonomous knockdown versus systemic mono-allelic disruption of *CHD8*). In addition, these two studies are mostly based on pulse-chase incorporation of a nucleotide analog, an approach that can only provide indirect, population-wide information about cell cycling parameters (Nowakowski et al., 1989).

To measure the direct influence of CHD8 on the cell cycle of human neural progenitors, we generated a stem cell model of *CHD8* haploinsufficiency by CRISPR/Cas9 gene editing and monitored cell cycle progression of individual NPCs with the fluorescent ubiquitination-based cell cycle indicator FUCCI (Sakaue-Sawano et al., 2008) by time-lapse microscopy. Using an image analysis pipeline that reconstructs individual cell lineages during several rounds of cell division and measures duration of G1 and S/G2/M during each cycle, we show that heterozygous LoF of *CHD8* results in a marked shortening of G1. Further, we demonstrate that this curtailed G1 phase results from impaired repression of several pathways that drive entry into S phase. Our findings provide strong evidence for an inhibitory function of CHD8 in NPC proliferation and suggest a mechanism for macrocephaly in individuals with *CHD8* DNMs based on abnormal expansion of the progenitor pool in the developing neocortex.

RESULTS

Mono-allelic disruption of *CHD8* in hESCs by CRISPR/Cas9 gene editing

The human CHD8 gene encodes two transcripts with a different 5′ exonic structure (Fig. 1A). We designed two small guide RNAs (sgRNAs) against the first two conserved exons (Fig. 1A), cloned them into a gRNA-Cas9 expressing DNA plasmid and nucleofected these gRNA-Cas9 constructs into hESCs. After confirming successful editing of the *CHD8* locus using the surveyor assay (Fig. S1), we isolated individual clones by limited dilution (about 50 clones for each sgRNA) and sequenced a ∼500 bp genomic amplicon containing the predicted edited sites. We obtained 4 to 6 edited clones per sgRNA indicating an editing frequency of ∼10%. To identify clones with a putative LoF indel, we analyzed DNA sequences displaying a clear breakpoint with the tracking of indels by decomposition (TIDE) software (Brinkman et al., 2014). TIDE identified several clones with a predicted mono-allelic indel (not shown). Based on TIDE's analysis, we selected clone E11 for further studies. For E11, TIDE predicted a heterozygous 1 bp insertion in exon 4 at the predicted double strand break (not shown). We confirmed TIDE's results by single-allele sequencing of E11 (Fig. 1B). Out of the 34 alleles we sequenced, 15 were wild type (wt) and 19 contained the 1 bp insertion (Fig. 1C), consistent with a heterozygous mutation. The frameshift induced by this 1 bp insertion resulted in the introduction of a stop codon 8 bp downstream of the mutation (Fig. 1D). Next, we quantified *CHD8* transcripts levels in wt and E11 hESCs using RT-qPCR. Two sets of TaqMan probes were used (Fig. 1A) annealing across exon–exon boundaries shortly after the DSB (exon 4-5, proximal probe) or towards the end of the transcript (exon 36-37, distal probe). We measured a decrease in the *CHD8* message of 49±0.06% standard deviation (s.t.d.) and 34±0.15% (s.t.d.) in E11 with the proximal and distal primer sets respectively (Fig. 1E). At the protein level, CHD8 localizes to distinct foci in the nucleus, the number and intensity of which are significantly reduced in E11 hESCs (Fig. 1F, G) – the mean nuclear intensity is decreased by 43±19% (s.t.d.) in the mutant line. Collectively, these results show successful disruption of one copy of the *CHD8* gene in the E11 hESC line. The E11 clone expressed the pluripotent stem cell marker Oct4 in virtually all cells, similar to wt hESCs (Fig. 2A,B; Fig. S2A) indicating that mono-allelic disruption of *CHD8* has not compromised the pluripotent state of these cells. We therefore used the E11 line as a stem cell model of *CHD8* haploinsufficiency in subsequent experiments.

Heterozygous disruption of *CHD8* increases the proportion of cells in G2/M at the expense of G0-G1

hESCs were next differentiated into NPCs using a neural induction procedure based on dual-SMAD inhibition (Gerrard et al., 2005; Chambers et al., 2009; Muratore et al., 2014). This protocol efficiently converts hESCs into NPCs of the dorsal telencephalon (forebrain) lineage, which progressively acquire the features of radial glial cells – the main source of neural stem cells in the developing cortex. We confirmed efficient differentiation of hESCs into NPCs by the concomitant loss of the pluripotent stem cell marker Oct4 and acquisition of the cortical progenitor marker Pax6 (Fig. 2A-D; Fig. S2A,B). Neural induction was quasi-complete for both $CHD8^{+/+}$ and $CHD8^{+/-}$ (E11) lines and led, at a later stage of differentiation, to the spontaneous assembly of neural rosettes (Fig. S2C), a defining behaviour of cortical progenitor cells (Ziv et al., 2015). To determine whether CHD8 influences the cell cycle, we first measured the distribution of cells in G0-G1, S and G2-M by flow cytometry (Fig. 2E-I). In hESCs, heterozygous disruption of *CHD8* led to a modest decrease in the fraction of cells in G0-G1 and a corresponding increase in the number of cells in G2-M (Fig. 2F,G). A similar but more pronounced effect was observed in NPCs (Fig. 2H,I). As expected, a higher fraction of NPCs were in G1 compared to hESCs (Fig. 2F,H) consistent with a longer G1 phase in neural progenitors (Calegari et al., 2005; Lange et al., 2009). These data show that a higher proportion of $CHD8^{+/-}$ NPCs and, to a lesser extent, $CHD8^{+/-}$ hESCs, are in G2-M, suggesting that these mutant cells proliferate faster.

Imaging cell cycle progression reveals marked shortening of G1 phase in $CHD8^{+/-}$ NPCs

To directly measure duration of cell cycle phases, we imaged cell cycle progression using FUCCI (Sakaue-Sawano et al., 2008) by dual-color live-cell confocal microscopy. This probe labels G1 phase nuclei in red and those in S/G2/M phases in green (Fig. 3A-C) without interfering with cell cycle dynamics (Pauklin and Vallier, 2013). To faithfully compare cell cycle progression in *CHD8* wt and mutant cells, both groups were simultaneously imaged in multiple wells of a 96-well plate for 20 to 70 h, by high-content microscopy. FUCCI was introduced in these cells by lentiviral delivery using a viral titer that led to 10-20% of FUCCI-expressing cells to allow tracking of individual cell lineages (Fig. S2A). Cells remained healthy and proliferative throughout the imaging session, as judged by a clear increase in colony size with time (Fig. S3B,C). The size of these data sets precluded manual analysis of cell cycle timing. Full automatization of cell tracking is difficult, however, because during conversion from green to red (M-G1), FUCCI emits no or little light for several successive frames (Fig. 3C-E). We thus wrote an interactive image processing algorithm that segments a cell and its progeny based on mouse clicks and plots dual-color fluorescent

Biology Open (2022) 11, bio058941. doi:10.1242/bio.058941

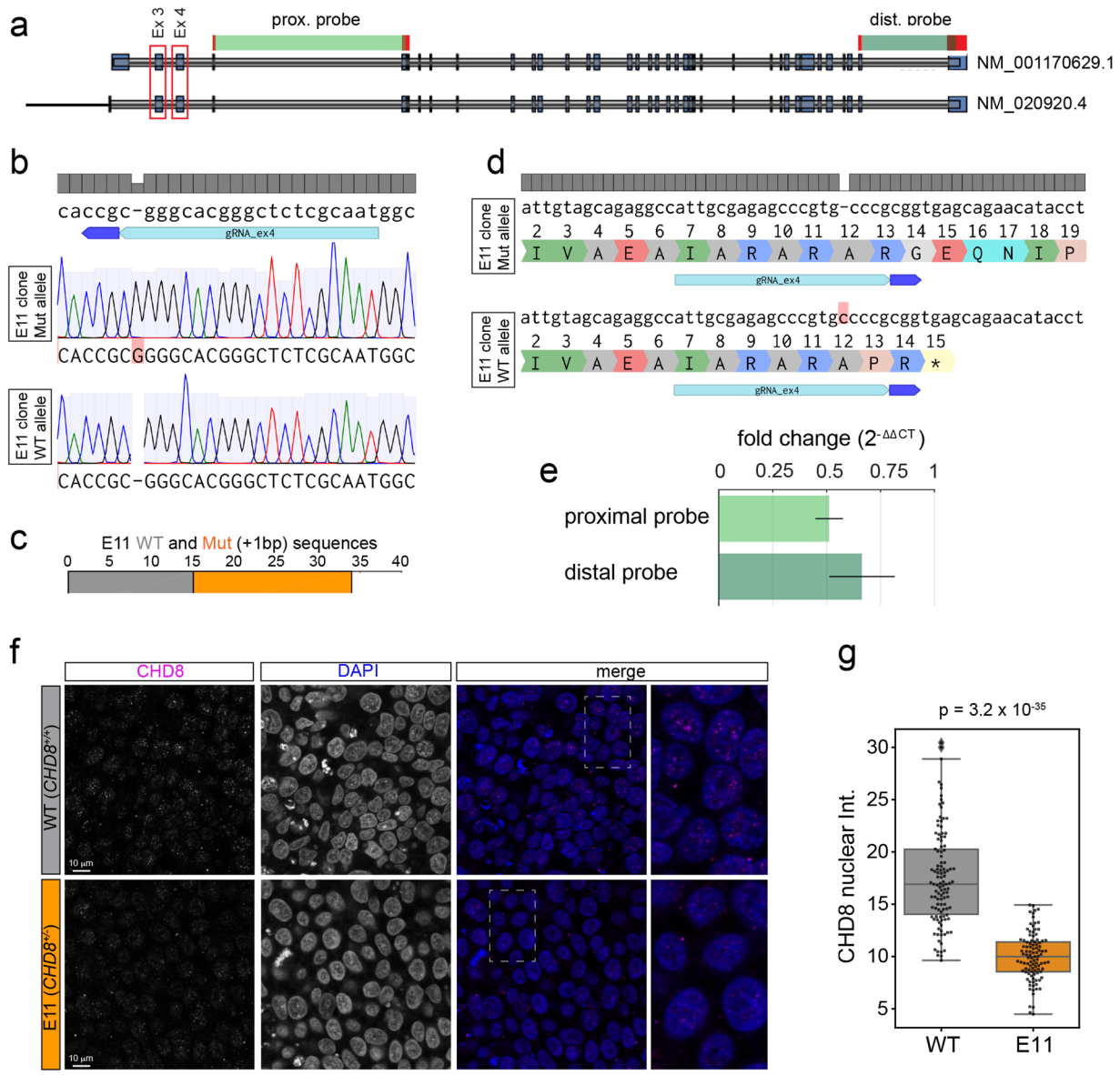

Fig. 1. Disruption of a single allele of *CHD8* in hESCs by CRISPR/Cas9 gene editing. (A) Genomic organization of the *CHD8* locus. Boxed in red are the first two conserved exons of the two *CHD8* variants against which sgRNAs were designed. The regions across exon–exon boundaries amplified by proximal and distal TaqMan primers are indicated in green. (B) Single-allele sequencing reveals the insertion of a single nucleotide C (G in the opposite strand sequenced here) at a frequency consistent with a heterozygous mutation (C). (D) DNA and protein sequence alignments of the wt (top) and mutated (bottom) allele of the E11 clone. The one base pair insertion introduces a stop codon shortly after the edited site. (E) TaqMan RT-qPCR showing fold-change in the *CHD8* mRNA transcript in E11 relative to wt hESCs (n=3). Error bars indicate s.t.d. (F,G) Immunofluorescence staining of CHD8 in WT and E11 hPSCs. (G) Quantification of CHD8 fluorescence intensity in individual nuclei of wt (n=114) and E11 (n=101) hPSCs. P-value was obtained by an unpaired t-test.

traces for mother and daughter cells (see Materials and Methods). G1 and S/G2/M lengths were then computed based on these time series (Fig. 3C). We estimate that this computer-assisted approach speeds up the analysis by a factor ∼10.

Using this image analysis pipeline, we first examined cell cycle timing in hESCs. *CHD8*$^{+/+}$ and *CHD8*$^{+/-}$ hESCs went through G1 in less than 3 h while they spent at least 10 h in S/G2/M (Fig. 3D-H). A short G1 phase with no apparent regulation of the G1 checkpoint is a hallmark of embryonic pluripotent stem cells (Pauklin and Vallier, 2013; Neganova et al., 2009, 2011). Accordingly, we rarely captured a clear G1/S transition in these cells (regardless of genotype), as reflected by little or no overlap between mKO2-Cdt1$_{30\text{-}120}$ and mAG-Geminin$_{1\text{-}110}$ expression (Fig. 3C). Occasionally, transient co-expression of mKO2-Cdt1$_{30\text{-}120}$ and mAG-Geminin$_{1\text{-}110}$ could be detected in wt but not in mutant cells (Fig. 3D-G). Notably, however, G1 length was shorter in *CHD8*$^{+/-}$ cells compared to their *CHD8*$^{+/+}$ counterparts – median±s.t.d. of 153±61 min versus 198±78 min (P=0.014) – (Fig. 3H), indicating that this phase of the cell cycle is further truncated in mutant cells. No significant difference in S/G2/M timing was observed between the two genotypes, although the relatively short duration of this live-cell experiment (20 h) precluded a precise comparison of S/G2/M lengths.

Next, we imaged cell cycle progression in stem-cell-derived neural progenitors for up to 3 days (70 h). We were able to track individual cell lineages in both wt and mutant hNPCs over several rounds of cell division (Fig. 4A-D). NPCs were more motile than their undifferentiated precursors, displayed a characteristic boomerang-shaped nucleus (Fig. 4A,B) and, as expected,

Biology Open (2022) 11, bio058941. doi:10.1242/bio.058941

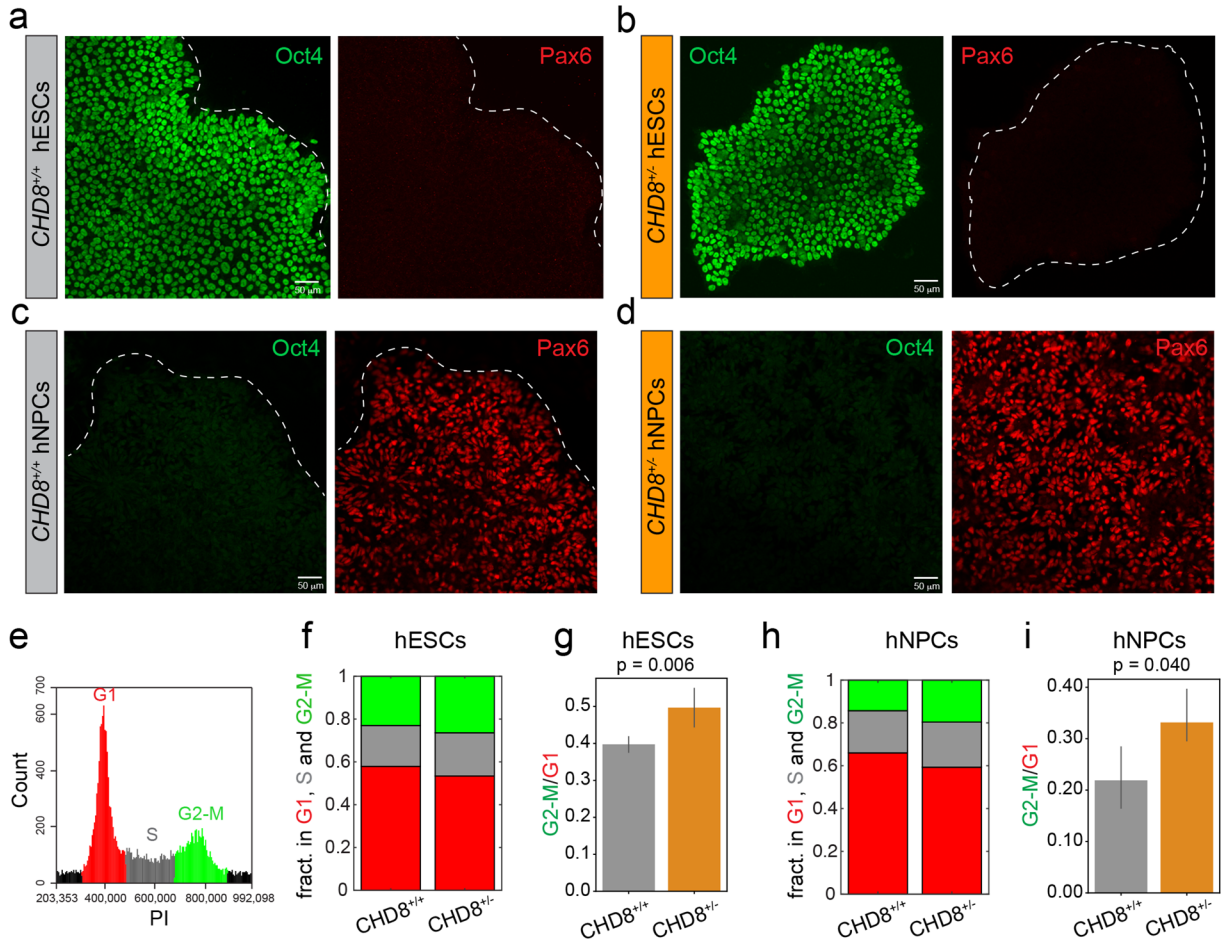

Fig. 2. Flow cytometry reveals subtle differences in cell cycle profile of *CHD8*$^{+/-}$ hESCs and hNPCs. (A-D) Immunostaining of Oct4 (green) and Pax6 (red) in *CHD8*$^{+/+}$ (A,C) and *CHD8*$^{+/-}$ (B,D) hESCs (A,B) and hNPCs (B,D). (E-I) Cell cycle profile by DNA content analysis. (E) PI Histogram of wt hESCs (cell number versus PI intensity) showing the distribution of cells in G0-G1, S and G2-M. (F,H) fraction of wt and mutant cells in G0-G1, S and G2/M for hESCs (F) and hNPCs (H). (G,I) Mean G2-M/G1-G0 ratio for hESCs (G) and hNPCs (I). *n*=3, error bars indicate 95% CI. *P*-values obtained by Mann–Whitney *U*-test.

progressed more slowly through the cell cycle (Fig. 4E). G1 in particular was significantly longer in hNPCs than in hESCs – up to 10× in wt cells (compare Figs 4E and 3H). G1/S transitions (overlapping green and red FUCCI signals) were also protracted in hNPCs consistent with the presence of a proper G1/S checkpoint in these cells. Comparative analysis of phase duration across genotypes revealed a marked shortening of G1 in *CHD8*$^{+/-}$ hNPCs compared to their wt counterparts – median±s.t.d. of 517±410 min versus 1408±982 min (P=7×10^{-7}) (Fig. 4C-E). In contrast, no overt change in S/G2/M duration was observed in mutant cells (Fig. 4C-E) indicating a profound and specific effect of *CHD8* haploinsufficiency on the G1 phase of the cell cycle. Collectively, these imaging experiments show that disruption of one *CHD8* copy is sufficient to severely shorten G1 and facilitate the G1/S transition in hNPCs, an effect that likely boosts proliferation of neural progenitors and delays their differentiation into neurons. Hence, CHD8 represses proliferation and self-renewal of hNPCs by lengthening G1 and the G1/S transition.

CHD8 represses pathways regulating S phase entry

To explore the mechanisms by which CHD8 lengthens G1, we searched for CHD8 target genes that regulate G1 and the G1/S checkpoint. Cyclins E1 and E2 are expressed during the G1/S transition and have been proposed to drive S phase entry. The expression of both E cyclins is modulated by CHD8, but the directionality of this regulation appears to be context-dependent (Rodríguez-Paredes et al., 2009; Shingleton and Hemann, 2015). A comparative RT-qPCR analysis showed that cyclin E1 (CCNE1), and to a lesser extent cyclin E2 (CCNE2), are upregulated in *CHD8*$^{+/-}$ hNPCs, while as expected, *CHD8* transcripts levels were halved (Fig. 5A). Elevated expression of cyclins E1 and E2 in mutant hNPCs is consistent with faster progression of these cells through the G1/S checkpoint and, thus, shorter G1. EGF-family growth factors and downstream MAPK activation is another key pro-mitotic signaling cascade regulating S phase entry (Kobayashi et al., 1998). Recently, *kismet*, the fly ortholog of mammalian *CHD7* and *CHD8,* was shown to downregulate the EGF receptor (EGFR) by upregulating transcription of the E3 ligase Cbl known to promote degradation of the EGFR (Gervais et al., 2019). To determine whether CHD8 transcriptionally regulates EGF signaling in neural progenitors, we first compared expression of Cbl in *CHD8*$^{+/-}$ and *CHD8*$^{+/+}$ hNPCs. In mammalian cells, two closely-related Cbl isoforms – Cbl and Cbl-b – have been implicated in EGFR degradation (Mohapatra et al., 2013). While Cbl expression is not influenced by CHD8, Cbl-b transcripts levels were 20% down in *CHD8*$^{+/-}$ hNPCs (Fig. 5A) indicating a mild repressive activity of CHD8. We next examined the impact of CHD8 on MAPK signaling. Immunostaining against a phosphorylated form of

Biology Open (2022) 11, bio058941. doi:10.1242/bio.058941

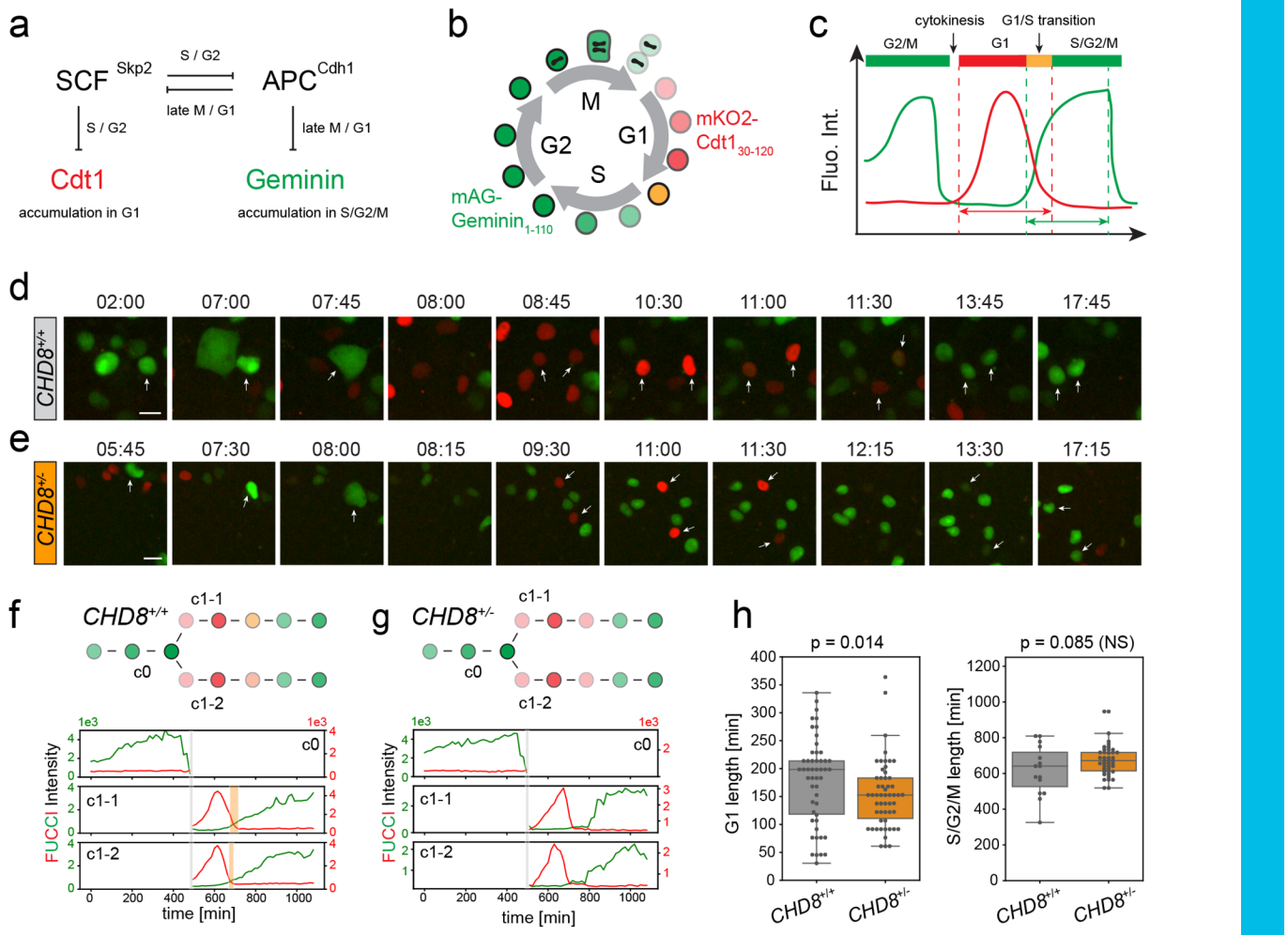

Fig. 3. Minimal perturbation of cell cycle timing in *CHD8*$^{+/-}$ hESCs. (A,B) Color-based detection of G1 and S/G2/M by the FUCCI fluorescent reporter. The G1 and S/G2/M probes are expressed as a single open reading frame using the T2A self-cleaving peptide sequence ensuring stochiometric expression of both probes. (C) Measurement of G1 and S/G2/M duration based on FUCCI intensity traces (see Materials and Methods). (D-H) High-content FUCCI imaging in wt (d,f,h) and mutant (e,g,h) hESCs. (D,E) Snapshots of *CHD8*$^{+/+}$ (D) and *CHD8*$^{+/-}$ (E) hESCs during cell cycle progression (~17 h). White arrows show a cell initially in S/G2 undergoing mitosis and cytokinesis and its two daughter cells transitioning from G1 to S/G2. Time is in h and min. Scale bar: 20 µm. (F,G) FUCCI intensity traces of mother and daughter cells marked by an arrow in D and E. The green y axis (left) indicates mAG-Geminin$_{1-110}$ intensity (S/G2/M), the red y axis (right) indicates mKO2-Cdt1$_{30-120}$ intensity (G1). Grey bars indicate cytokinesis (M/G2). Orange bars indicate G1/S transitions. (H) Box plots showing duration of G1 and S/G2/M in *CHD8*$^{+/+}$ (*n*=48) and *CHD8*$^{+/-}$ (*n*=49) cells. *P*-values were measured using a Mann–Whitney *U*-test.

ERK1/2 (Thr202/Tyr204) revealed a marked increase in the activity of this MAPK in *CHD8*$^{+/-}$ hNPCs, particularly in the nucleus (Fig. 5B,D,E). Total levels of Erk were not significantly changed in mutant cells (Fig. 5C,F). Together, these results show that CHD8 represses two central signaling pathways that regulate progression through G1. Disruption of one *CHD8* allele is sufficient to relieve this transcriptional inhibitory circuit and accelerate S phase entry in neural progenitors (Fig. 6).

DISCUSSION

Cell cycle timing is of central importance for organ growth and maintenance. Changes in duration of cell cycle phases, G1 in particular, have been proposed to control the balance between stem cell proliferation and differentiation and are thought to play instructive roles in cell fate decisions at different stages of development – from the original differentiation of ESCs into the three primary germ layers (Pauklin and Vallier, 2013) to the final assembly of organs including the brain (Dehay and Kennedy, 2007). ESCs and PSCs typically have a short G1 phase which reflects the lack of a proper G1/S checkpoint. Differentiation of stem cells is invariably associated with lengthening of G1, a process thought to broaden the receptive window of these cells to extrinsic cues. Increase in G1 duration is also observed in the mammalian developing cortex, as progenitors transition from proliferative to neurogenic modes of cell division (Calegari et al., 2005; Lange et al., 2009).

In agreement with these findings, we observed a pronounced lengthening of G1, up to tenfold in wt cells, after differentiation of hESCs into hNPCs, with no overt change in other phases of the cell cycle (Figs 3 and 4). The median G1 duration in wt hNPCs is particularly long (29 h) and is characterized by a large variance across individual cells (Fig. 4E), possibly reflecting cell cycle exit and re-entry events (Dehay and Kennedy, 2007; Pajalunga et al., 2008). G1 length only increases about three times in *CHD8*$^{+/-}$ NPCs relative to their undifferentiated precursors and is also about three times shorter than that of their *CHD8*$^{+/+}$ counterparts. Given that the median difference in G1 between wt and mutant NPCs is ~15 h (900 min), this truncated G1 phase results in more than a twofold shortening of the cell cycle in *CHD8*$^{+/-}$ NPCs. Halving the

Biology Open (2022) 11, bio058941. doi:10.1242/bio.058941

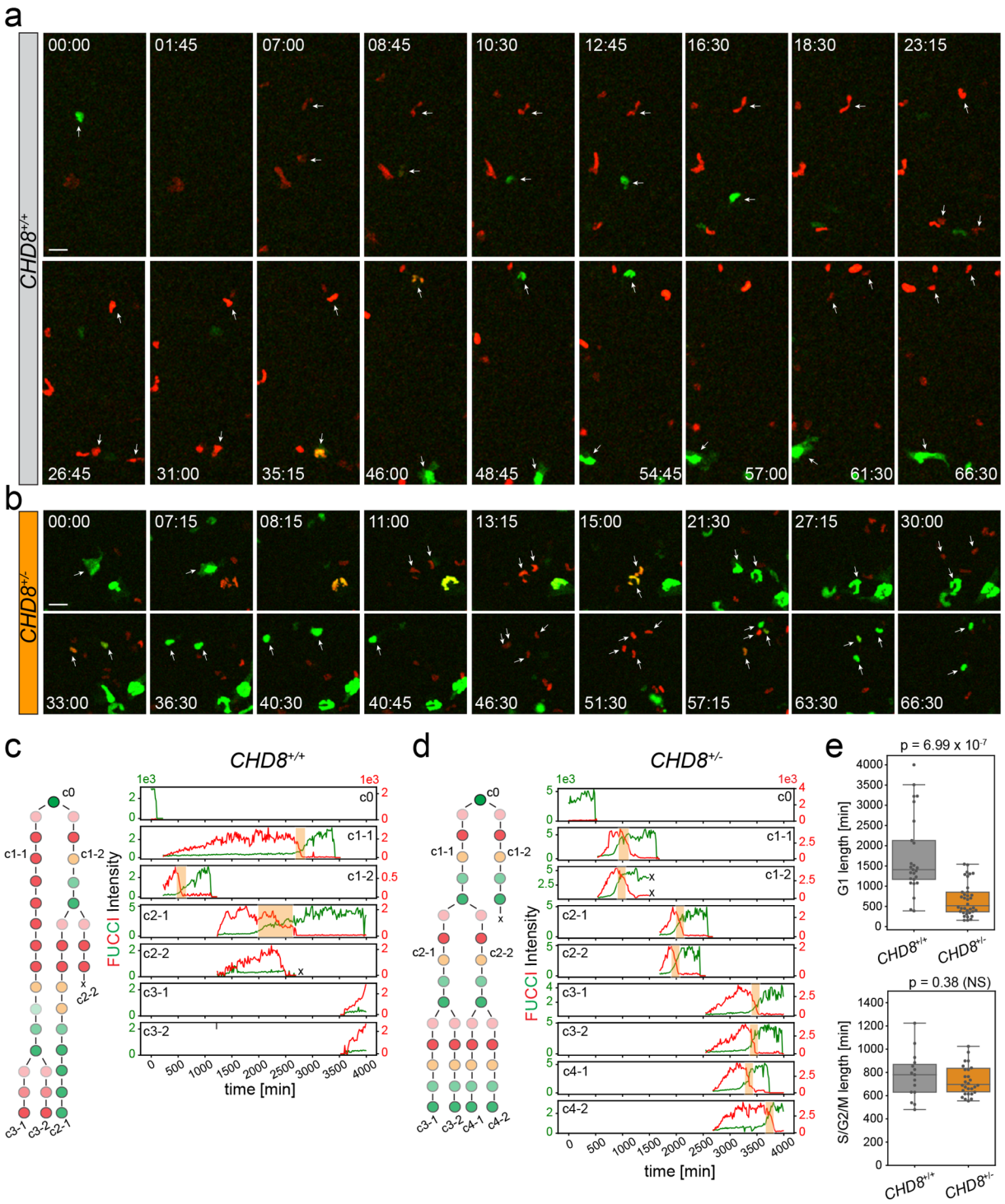

Fig. 4. Marked reduction of G1 length in *CHD8*$^{+/-}$ hNPCs. (A,B) Time-lapse imaging of clonal lineages in wt (A) and mutant (B) NPCs going through several rounds of cell division over the course of ∼70 h. Cells corresponding to a single lineage are marked by white arrows. Time is indicated in h and min. Scale bar: 20 µm. (C,D) Lineage reconstruction and FUCCI intensity traces of individual cells marked by an asterisk in A and B for wt (C) and mutant (D) NPCs. The green y axis (left) indicates mAG-Geminin$_{1\text{-}110}$ intensity (S/G2/M), the red y axis (right) indicates mKO2-Cdt1$_{30\text{-}120}$ intensity (G1). Orange bars show G1/S transitions. (E) Box plots show duration of G1 and S/G2/M in *CHD8*$^{+/+}$ (*n*=23) and *CHD8*$^{+/-}$ (*n*=34) cells. *P*-values were measured using a Mann–Whitney *U*-test.

length of the cell cycle is predicted to double the size of the progenitor pool and the rate of neuron production (Caviness et al., 2003), an effect that should lead to a substantial increase in the number of cortical neurons in the adult brain. A threefold shortening of G1 in progenitors is also expected to severely affect the balance between proliferation and differentiation. G1 shortening by overexpression of Cdk4/cyclinD1 promotes expansion of mouse progenitors and delays neurogenesis (Lange et al., 2009). This, together with other reports indicating shortening of G1 in cortical progenitors exposed to mitotic cues and, conversely, increase in

Biology Open (2022) 11, bio058941. doi:10.1242/bio.058941

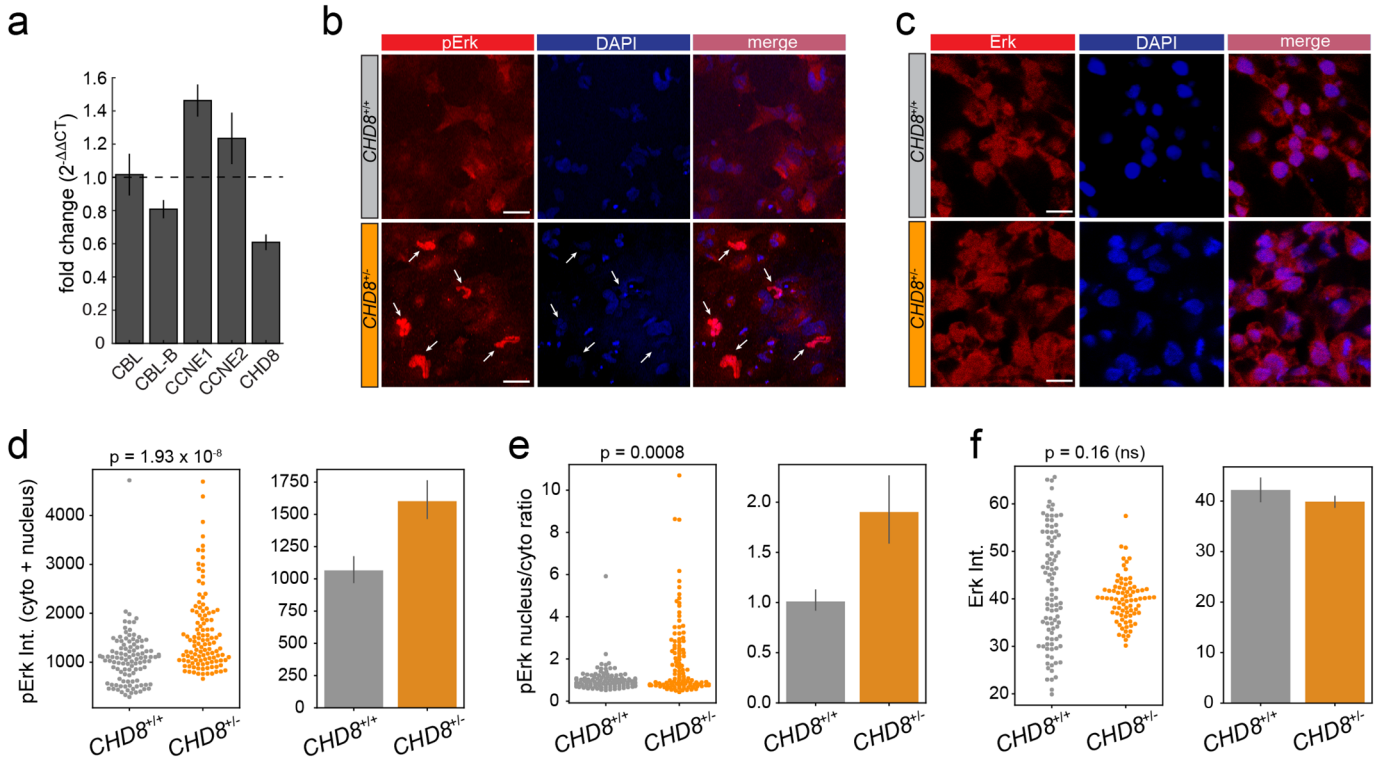

Fig. 5. CHD8 represses cyclins E and MAPK signaling. (A) RT-qPCR analysis of *CHD8*$^{+/+}$ and *CHD8*$^{+/-}$ hNPCs. Fold-change (mut/wt) in mRNA expression is shown for the indicated genes (n=4, error bars indicate s.t.d.). (B,C) pErk (B) and Pan-Erk (C) immunostaining in *CHD8*$^{+/+}$ and *CHD8*$^{+/-}$ hNPCs. Arrows point to pERK in the nucleus. Scale bar: 20 µm. (D,E) Quantification of pERK total intensity (D) and nucleus to cytoplasm intensity ratio (E) in *CHD8* wt (*n*=109) and mutant cells (*n*=116). (F) Quantification of total Erk intensity in *CHD8* wt (*n*=97) and mutant (*n*=80) cells. Intensity data are visualized in swarmplots and bar graphs (mean Intensity±95% CI). *P*-values were measured using a Mann–Whitney *U*-test.

G1 length by differentiation factors (Lukaszewicz et al., 2002), suggest that cell cycle timing may influence the switch from self-renewing to neurogenic divisions. Based on these data, it is tempting to speculate that shortening of G1 in CHD8$^{+/-}$ NPCs promotes proliferative divisions at the expense of neurogenic ones thus further contributing to the expansion of the neural progenitor pool. This model also predicts delayed neuronal differentiation and maturation in *CHD8*$^{+/-}$ developing cortices, a form of neoteny recently described in both mouse and iPSC models of *CHD8* haploinsufficiency (Gompers et al., 2017; Liu et al., 2019 preprint), and other animal models of autism (Chomiak and Hu, 2013). Together, our findings support the notion that macrocephaly in the CHD8 ASD subtype (and in animal models of CHD8 haploinsufficiency) results primarily from an accelerated expansion of the neural progenitor pool.

How does CHD8 prolong the G1 phase of the cell cycle? We provide evidence that CHD8 represses two key pathways that regulate progression through G1 and S phase entry. Disruption of one copy of *CHD8* results in transcriptional upregulation of E cyclins, cyclin E1 in particular. E cyclins are turned on in late G1 and together with their cognate cyclin-dependent kinase cdk2 regulate G1/S checkpoint transition in ESCs (Neganova et al., 2009; Neganova et al., 2011) and cortical progenitors (Delalle et al., 1999; Lukaszewicz et al., 2005; Watanabe et al., 2015). This inhibitory effect of CHD8 on E cyclins expression is in good agreement with a recent RNAseq study in *CHD8*$^{+/-}$ iPS-derived cerebral organoids (Wang et al., 2017) but contrasts with an earlier report in HeLa cells showing an opposite effect of CHD8 on cyclin E transcription (Rodríguez-Paredes et al., 2009). These seemingly contradictory results probably reflect context-dependent transcriptional regulation by CHD8 (Durak et al., 2016), a feature particularly apparent in cancer, where CHD8 has been proposed to operate as a tumor suppressor in some malignancies and a proto-oncogene in others (Shingleton and Hemann, 2015). In addition, we show that *CHD8* haploinsufficiency causes a mild downregulation of Cbl-b transcription – an E3 ligase implicated in degradation of the EGFR – and a marked upregulation of Erk phosphorylation, indicating a repressive action of CHD8 on MAPK activity. The small decrease in Cbl-b mRNA levels (20%) does not scale up with the potent increase in Erk phosphorylation observed in *CHD8*$^{+/-}$ suggesting that CHD8 interferes with MAPK signaling in multiple ways. The MAPK pathway operates in early G1 and is essential for (re)-entry into mitosis (Liu et al., 2004). Upregulation of MAPK activity in *CHD8*$^{+/-}$ may therefore also drive cell cycle re-entry in a subset of quiescent NPCs, further accelerating G1 in mutant progenitors.

Collectively, our findings provide compelling evidence for dysregulated proliferation of neural progenitors in *CHD8*$^{+/-}$ developing brains and strengthen the unexpected connection between autism and cancer (Crawley et al., 2016). Several other autism risk factors are also associated with cancer, including PTEN, and components of the mTOR and Ras-MAPK pathways. PTEN-ASD is estimated to represent up to 2% of all autism cases (Crawley et al., 2016) and is also strongly associated with macrocephaly (Varga et al., 2009). Of note, 27% of people with RASopathies – a group of five neurodevelopmental disorders caused by mutations in the Ras-MAPK pathway that all result in Erk gain-of-function – meet the criteria for autism (Adviento et al., 2014). Our work thus identifies MAPK signaling as a potential therapeutic target for the treatment of the CHD8 ASD subtype and suggests that cancer drugs targeting the MAPK pathway may be therapeutically active in idiopathic autism.

Biology Open (2022) 11, bio058941. doi:10.1242/bio.058941

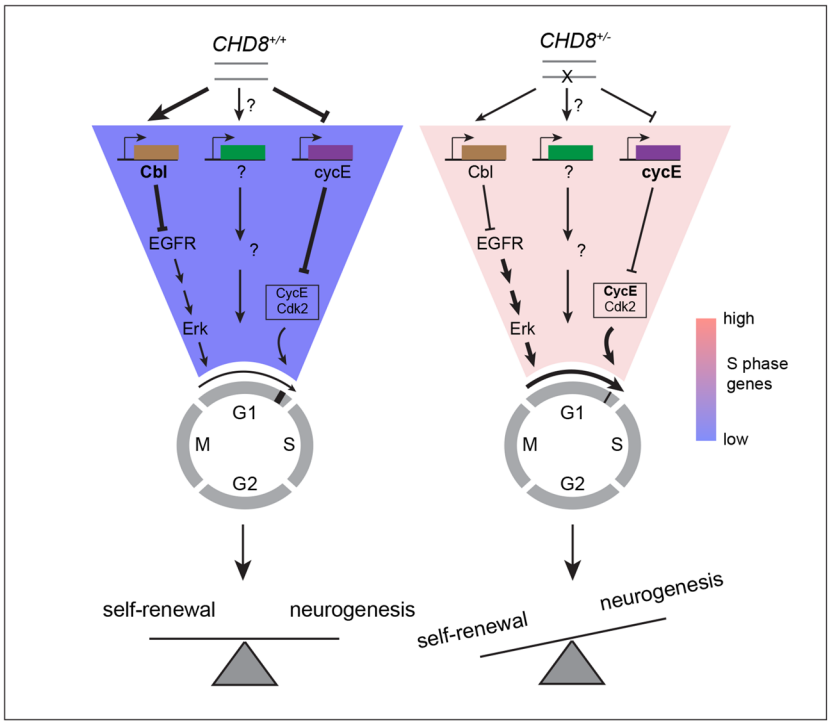

Fig. 6. A model for CHD8 regulation of G1 length and S phase entry. Loss-of-function of a single *CHD8* allele shortens the G1 phase of the cell cycle in neural stem cells by relieving transcriptional repression of the MAPK pathway and cyclins E. Truncated G1 causes overproliferation of cortical progenitors by accelerating the cell cycle and by promoting self-renewing divisions at the expense of neurogenic ones.

MATERIALS AND METHODS

DNA constructs, antibodies and other reagents

The pSpCas9(BB)-2A-Puro (PX459) V2.0 (#62988), pBOB-EF1-FastFUCCI-Puro (#86849), psPax2 (gag-pol) (#12260) and pMD2.G (vsvg) (#12259) DNA plasmids were from addgene. The Pax6 rabbit pAb (Poly19013) was from BioLegend. The OCT4 mouse mAb (3A2A20) was from StemCellTech. The rabbit Phospho-p44/42 MAPK (Erk1/2) (Thr202/Tyr204) mAb (4370) was from CST. The polyclonal rabbit p44/42 MAPK (Erk1/2) Ab was from CST (4695). The rabbit polyclonal Ab to CHD8 (ab224830) was from abcam. All secondary Abs were from Thermo Fisher Scientific: goat anti-rabbit IgG Alexa Fluor 555 (A27039) and goat anti-mouse IgG Alexa Fluor 488 green (A-11001).

Maintenance and differentiation of hESCs

The hESCs line H9 (WA09) was from WiCell. We obtained authorization from WiCell (MTA) and from the UK Stem Cell Bank to import and use this line in our laboratory. All stem cell culture reagents were from STEMCELL technologies. We maintained and differentiated hESCs according to STEMCELL protocols.

Maintenance

hESCs were grown in mTeSr™ medium on matrigel-coated in (Geltrex A1413201, Thermo Fisher Scientific) tissue-culture-treated six-well plates (Corning). Medium was changed daily. hESCs were passaged every 5-7 days using the ReLeSR™ dissociation reagent. Care was taken to passage cells as colonies before they reached confluency. For nucleofection and differentiation, hESCs were dissociated to the single-cell level using the GCDR dissociation reagent and grown in the appropriate medium containing 10 µM Y-27632 (ROCK inhibitor) for the first 24 h after dissociation. hESCs were cryopreserved in mFreSR™ and thawed in mTeSr™ containing 10 µM Y-27632 for 12-24 h until the colonies reached a sufficient size.

Differentiation

hESCs were dissociated to the single-cell level and grown in STEMdiff™ neural induction media containing dual SMAD inhibitors, in the presence of Y-27632 (10 µM) for the first 24 h. Medium was changed daily. Cells were passaged a first time after ∼7 days using accutase, grown for another ∼7 days in STEMdiff™ (+ dual SMADi) neural induction media and passaged a second time with accutase into STEMdiff™ neural progenitor medium (containing supplements A and B) for final differentiation into NPCs. NPCs were used for experiments after at least one passage in STEMdiff™ neural induction medium. At this point, >90% NPCs stained positive for Pax6 and negative for Oct4. For all experiments comparing the behavior $CHD8^{+/+}$ and $CHD8^{+/-}$ NPCs, cells from these two groups were differentiated in parallel and examined after the exact same number of passages.

CRISPR/Cas9 gene editing in hESCs

sgRNA design, cloning and transfection

20-mer sgRNA were designed using the CRISPR design tool [http://crispr.mit.edu/] against exons 3 and 4 of *CHD8* – the first two conserved exons of the two *CHD8* variants (RefSeq accession numbers NM_001170629.2 and NM_020920.4). We selected two sgRNAs (one against each exon) with the highest score. We then used a plasmid-based procedure for scarless cloning of double-stranded oligonucleotides encoding the sgRNA and its complementary sequence into a cassette containing Cas9 and the sgRNA's scaffold (Ran et al., 2013). Forward and reverse oligos for each gRNA contained overhangs for directional cloning into the pSpCas9(BB)-2A-Puro plasmid using the BBS1 restriction site. These oligos contained an additional G-C pair upstream of the 20nt gRNA sequence to enhance transcription by the vector's U6 promotor (Ran et al., 2013). Forward and reverse oligos were phosphorylated with T4 polynuclease kinase, annealed to form dsDNA, and the DNA duplex was cloned into pSpCas9(BB)-2A-Puro by restriction digest with BBS1 and ligation using T4 ligase. Ligation products were then transformed into Sbtl3 competent bacteria. Proper insertion of the sgRNA sequences was confirmed by Sanger sequencing. gRNA-Cas9 constructs were then separately introduced in hESCs using the Amaxa 4D-nucleofector (Lonza) and the nucleofection program/kit designed for the H9 hESC line. For this, hESCs were dissociated at the single cell level and deposited in a 16-well Nucleocuvette strip in presence of the ROCK inhibitor Y27632 (200,000 cells per well) and 2 µg of ex3-gRNA-Cas9 or ex4-gRNA-Cas9 or control plasmids containing the Cas9-expressing vector without sgRNA or a GFP-expressing plasmid to evaluate transfection efficiency. We typically obtained 60-70% transfection efficiency using this protocol. Cells were immediately transferred to a 24-well plate after electroporation and grown for another 24 h in presence of Y27632.

Biology Open (2022) 11, bio058941. doi:10.1242/bio.058941

Table 1. DNA oligos for sgRNA cloning, genomic PCR and single-allele sequencing

Name	Application	Sequence (5′ to 3′)	Length
CHD8_ex3_gRNA_fwd	sgRNA clon.	CACCGGACATCGGCATGTTGTGCTA	25
CHD8_ex3_gRNA_rev	sgRNA clon.	AAACTAGCACAACATGCCGATGTCC	25
CHD8_ex4_gRNA_fwd	sgRNA clon.	CACCGATTGCGAGAGCCCGTGCCCG	25
CHD8_ex4_gRNA_rev	sgRNA clon.	AAACCGGGCACGGGCTCTCGCAATC	25
CHD8_ex3_surv_fwd	Gen. PCR/seq (EcoRI)	ATGCGAATTCTGCAGTACCACCTTGACTGG	30
CHD8_ex3_surv_rev	Gen. PCR (HindIII)	CATAAGCTTAGTTGTACTGTGTCTTCTGACCTG	33
CHD8_ex4_surv_fwd	Gen. PCR/seq (EcoRI)	ATGCGAATTCAGCACTCTTCTTCCTGCGTT	30
CHD8_ex4_surv_rev	Gen. PCR (HindIII)	CATAAGCTTTCTGAGCTTGATTCTTGAGGG	30
M13R	Seq primer	CAGGAAACAGCTATGACC	18

Surveyor assay

Indel frequency was assessed using the surveyor assay (Integrated DNA Technologies, IDT) according to the manufacturer's instructions. ∼500 bp genomic DNA fragments encompassing the predicted DSB in both exon 3 and 4 were amplified from nucleofected hESCs using primers described in Table 1. These genomic amplicons were then denatured, re-annealed and digested with the mismatch-specific surveyor endonuclease. The digestion patterns we obtained from hESCs transfected with ex3-gRNA-Cas9 and ex4-gRNA-Cas9 constructs are consistent with the presence of indels at the site predicted by the sgRNA sequence (Fig. S1A in Data). These digested PCR products were not observed in hESCs transfected with a GFP plasmid (Fig. S1A).

Isolation of single CRISPR clones

After confirmation of successful editing by the surveyor assay, we isolated individual clones of hESCs by limited dilution in matrigel-coated 10 cm dishes (56.7 cm^2). Individual colonies were manually picked under the microscope and seeded in a 96-well plate for expansion and cryopreservation. For each sgRNA, about 50 clones were successfully expanded and screened for the presence of indels by DNA sequencing of a genomic amplicon. We used the same primers for genomic PCR and sequencing of a ∼500 bp region containing the predicted edited site in exon 3 and 4 (Table 1).

TIDE analysis and single-allele sequencing

Genomic amplicons originating from individual hESC clones were further analyzed by the TIDE software (Brinkman et al., 2014) for deconvolution of mixed sequences and prediction of indel type and frequency (www.tide.nki.nl). For single allele sequencing, genomic amplications (amplified with primers containing the HINDIII and ECOR1 sites, Table 1) were cloned by restriction digest into the pUC19 plasmid and sequenced using the M13R oligo (Table 1). More than 30 transformants were sequenced to obtain a reasonable estimate of mutation frequency.

TaqMan RT-qPCR

Total RNA was isolated from hESCs or NPCs grown in a six-well plate (9.5 cm^2) using the RNeasy minikit (Qiagen). A DNase 1 digestion step was performed during RNA extraction to degrade remaining genomic DNA. 2 µg total RNA was reverse-transcribed into cDNA using the high capacity cDNA reverse transcription kit (Thermo Fisher Scientific, 4368813). RT-qPCR was performed with Taqman assay chemistry in a 96-well format using a QuantStudio1 RT-qPCR machine (Applied Biosystems). TaqMan probes (Table 2) were pre-designed by Thermo Fisher Scientific across exon-exon boundaries. Fold-change in transcript expression was calculated using the $2^{-\Delta\Delta Ct}$ method. ΔCt was calculated by subtracting the Ct value of the control gene POLR2a from that of the target gene (probe). ΔΔCt was calculated by subtracting the ΔCt of the target gene (probe) in $CHD8^{+/+}$ (wt) cells from that in $CHD8^{+/-}$ (mutant) cells. Fold-change in gene expression is the average of three independent experiments (n=3). For each independent experiment, Ct was measured in triplicates or quadruplicates.

Flow cytometry

The distribution of hESCs and NPCs in the different phases of the cell cycle was measured by DNA content analysis using flow cytometry. hESCs or NPCs were cultured in matrigel-coated six-well plates (9.5 cm^2) until they reached ∼70% confluency, dissociated into a single-cell suspension, fixed with EtOH and stained with Propidium Iodide (ab139418, abcam) according to the manufacturer's instructions. $CHD8^{+/+}$ and $CHD8^{+/-}$ cells were then analyzed in parallel on a BD Accuri C6 flow cytometer. Cell debris and doublets were gated out using forward and side scatter density plots (FSC-A versus SSC-A) and forward scatter height versus forward scatter density area plots (FSC-A versus FSC-H), respectively. PI fluorescence was detected using the PE-A channel. PI histograms (cell count versus PI intensity) were then generated and gated to isolate G0-G1, S and G2-M phases (Fig. 2C). The percentage of cells in each of these three groups was then computed and averaged from three independent experiments comparing the two genotypes in hESCs and NPCs.

Lentiviral production

Low passage Hek293FT cells were grown in five T175 flasks in G1 medium (DMEM supplemented with 10% FBS, 1 mM sodium pyruvate, G418 and PenStrep). When cells reach 70-80% confluency, they were transfected with the following three DNA plasmids: pBOB-EF1-FastFUCCI-Puro, psPax2 (gag-pol) and pMD2.G (vsvg), at a 3:2:1 ratio using Lipofectamine 3000. 6 h post transfection cells were switched to Ultraculture medium (Lonza) and grown for another 24-48 h. The supernatant containing the viral particles was collected, cleared by low-speed centrifugation (1000 rpm for 5 min) and filtered on a 0.45 µm filter-flask. The filtered supernatant (∼120 ml) was then placed at the bottom of two conical centrifuge tubes, overlaid with 20 ml of 20% sucrose in PBS and spun at 20,000 ***g*** for 2 h at 4°C. The viral pellet was then resuspended in 1.5 ml ice-cold PBS from each centrifuge tube. Lentiviral particles were

Table 2. RT-qPCR TaqMan probes

Gene	Probe name	Description	Amplicon length
POLR2A	Hs00172187_m1	Housekeeping gene (control) (exons 1-2)	61
CHD8	Hs01025806_m1	Proximal probe (exons 4-5)	133
CHD8	Hs00394229_m1	Distal probe (exons 36-37)	78
Cbl-B	Hs00180288_m1	Cbl proto-oncogene B (exons 6-7)	98
Cbl	Hs01011446_m1	Cbl proto-oncogene or C-CBL (exons 5-6)	72
CCNE1	Hs00233356_m1	Cyclin E1/CCNE1 (exons 4-5)	101
CCNE2	Hs00180319_m1	Cyclin E2/CYCE2 (exons 6-7)	92

cleared by a final spin at 1000 ***g*** for 10 mins (4°C). The supernatant was alicoted (5 µl) and immediately frozen at −80°C.

Live-cell confocal imaging and analysis of cell cycle timing

Live-cell imaging was carried out in a temperature (37°C) and CO_2-controlled environment using a Micro Confocal high-content imaging system (Molecular Devices, USA) or laser-scanning confocal LSM 880 with airy scan (Zeiss, Germany).

Analysis of cell cycle timing

To extract cell cycle timing information from FUCCI time series, we developed a MATLAB-based interactive point-and-click segmentation algorithm. A binary image stack (time series) is first generated for each channel (green: mAG-Geminin$_{1\text{-}110}$, red: mKO2-Cdt1$_{30\text{-}120}$) using an adaptive thresholding approach. Color-specific binary stacks are then combined into a single stack which is used for click-based segmentation. Point-and-click is performed by the user on a merged RGB image of the green and red channels containing an interactive cursor to facilitate identification of cells. A cell and its progeny are then identified by a mouse click iteratively through the time series using the 'bwselect' function in matlab. The sequence of mouse clicks defines cell identity throughout the stacks allowing to build cell lineages. The mean green and red fluorescence intensity in each segmented and tracked nucleus is then recorded and plotted as a function of time. Cell cycle phase duration (G1 and S/G2/M) is then computed based on the green and red intensity profiles for each cell in a lineage. The matlab script required to run this analysis is available in the Materials and Methods.

Immunofluorescence

Cells were seeded on matrigel-coated glass coverslips, fixed with 4% paraformaldehyde, 4% sucrose for 20 mins, permeabilized with 0.5% Triton-X100 and blocked with 10% HSA (H0146, Thermo Fisher Scientific) and 1% BSA (15561020, Thermo Fisher Scientific) in PBS. Cells were incubated with primary antibodies (anti-CHD8 1:500, anti-pErk: 1/500, anti-Erk 1/500, anti-Pax6 1/1000 and anti-Oct4 1/1000 in PBS containing 1% BSA, briefly washed, and incubated with secondary Abs (1:1000) in PBS-BSA. After PBS wash, cells were mounted on glass slides with Mowiol (Sigma-Aldrich). Imaging was performed with an LSM 880 confocal microscope, (Zeiss, Germany). Laser intensity and gain were adjusted to prevent pixel saturation. All images comparing signal intensity were acquired using the same microscope configuration settings and visualized using identical contrast settings in ImageJ.

For analysis of pErk, Erk and CHD8 intensity, ROIs were manually drawn using ImageJ to segment individual nuclei or cells. Single-cell Mean intensities were exported and read into a panda dataframe using python (Jupyter Notebook). Mean fluorescent intensities of cell and nuclei populations were visualized using swarmplots, boxplots or bar graphs with the seaborn data visualization library.

Statistical analysis

Boxplots and swarmplots were generated with Python (Jupyter notebook) using the seaborn data visualization library. The box shows the quartiles (25% and 75%) of the dataset. The whiskers show the rest of the distribution contained within 1.5× the interquartile range (IQR). The median of the distribution is indicated by a horizontal bar. We used the Python SciPy library for statistical analysis. The nonparametric Mann-Withney *U* test was employed to compare cell cycle timing data and pErk expression in *CHD8*$^{+/+}$ and *CHD8*$^{+/-}$ cells. Unpaired *t*-test was used to compare CHD8 nuclear intensity in *CHD8*$^{+/+}$ and *CHD8*$^{+/-}$ hESCs. *P*-values were corrected for multiple hypothesis testing using the post-hoc Bonferroni method.

Acknowledgements

We thank Prof. Lauren Pecorino, Dr Yvonne Walsh and Patricia Lopez Garcia for critical reading of the manuscript. We are very grateful to Dr Andy Bashford (Molecular Devices) for giving us access to the ImageExpress MicroConfocal microscope for some of our imaging experiments.

Competing interests

The authors declare no competing or financial interests.

Conflict of interest

None. No part of this work is in any way relevant to or influenced by the main R&D objectives pursued by the biotech company. reMYND which now employs M.F.

Author contributions

Conceptualization: E.C.-Y., S.R., G.G., M.F.; Methodology: E.C.-Y., S.S., M.F.; Software: M.F.; Validation: E.C.-Y., M.F.; Formal analysis: E.C.-Y., M.F.; Investigation: E.C.-Y., M.R., S.S., M.F.; Resources: S.S., M.F.; Data curation: E.C.-Y., M.R., M.F.; Writing - original draft: M.F.; Writing - review & editing: M.F.; Visualization: E.C.-Y., M.F.; Supervision: S.R., G.G., S.S., M.F.; Project administration: S.R., G.G., S.S., M.F.; Funding acquisition: M.F.

Funding

This work was supported by a project grant from the Leverhulme Trust [RPG-2018-265] to M.F. https://dx.doi.org/10.13039/501100000275.

References

Adviento, B., Corbin, I. L., Widjaja, F., Desachy, G., Enrique, N., Rosser, T., Risi, S., Marco, E. J., Hendren, R. L., Bearden, C. E. et al. (2014). Autism traits in the RASopathies. *J. Med. Genet.* **51**, 10-20. doi:10.1136/jmedgenet-2013-101951

An, Y., Zhang, L., Liu, W., Jiang, Y., Chen, X., Lan, X., Li, G., Hang, Q., Wang, J., Gusella, J. F. et al. (2020). De novo variants in the Helicase-C domain of CHD8 are associated with severe phenotypes including autism, language disability and overgrowth. *Hum. Genet.* **139**, 499-512. doi:10.1007/s00439-020-02115-9

Barnard, R. A., Pomaville, M. B. and O'Roak, B. J. (2015). Mutations and modeling of the chromatin remodeler CHD8 define an emerging autism etiology. *Front. Neurosci.* **9**, 477. doi:10.3389/fnins.2015.00477

Bernier, R., Golzio, C., Xiong, B., Stessman, H. A., Coe, B. P., Penn, O., Witherspoon, K., Gerdts, J., Baker, C., Vulto-van Silfhout, A. T. et al. (2014). Disruptive CHD8 mutations define a subtype of autism early in development. *Cell* **158**, 263-276. doi:10.1016/j.cell.2014.06.017

Brinkman, E. K., Chen, T., Amendola, M. and van Steensel, B. (2014). Easy quantitative assessment of genome editing by sequence trace decomposition. *Nucleic Acids Res.* **42**, e168. doi:10.1093/nar/gku936

Calegari, F., Haubensak, W., Haffner, C. and Huttner, W. B. (2005). Selective lengthening of the cell cycle in the neurogenic subpopulation of neural progenitor cells during mouse brain development. *J. Neurosci.* **25**, 6533-6538. doi:10.1523/JNEUROSCI.0778-05.2005

Caviness, V. S., Goto, T., Tarui, T., Takahashi, T., Bhide, P. G. and Nowakowski, R. S. (2003). Cell output, cell cycle duration and neuronal specification: a model of integrated mechanisms of the neocortical proliferative process. *Cereb. Cortex* **13**, 592-598. doi:10.1093/cercor/13.6.592

Chambers, S. M., Fasano, C. A., Papapetrou, E. P., Tomishima, M., Sadelain, M. and Studer, L. (2009). Highly efficient neural conversion of human ES and iPS cells by dual inhibition of SMAD signaling. *Nat. Biotechnol.* **27**, 275-280. doi:10.1038/nbt.1529

Chomiak, T. and Hu, B. (2013). Alterations of neocortical development and maturation in autism: insight from valproic acid exposure and animal models of autism. *Neurotoxicol. Teratol.* **36**, 57-66. doi:10.1016/j.ntt.2012.08.005

Cotney, J., Muhle, R. A., Sanders, S. J., Liu, L., Willsey, A. J., Niu, W., Liu, W., Klei, L., Lei, J., Yin, J. et al. (2015). The autism-associated chromatin modifier CHD8 regulates other autism risk genes during human neurodevelopment. *Nat. Commun.* **6**, 6404. doi:10.1038/ncomms7404

Crawley, J. N., Heyer, W.-D. and LaSalle, J. M. (2016). Autism and cancer share risk genes, pathways, and drug targets. *Trends Genet.* **32**, 139-146. doi:10.1016/j.tig.2016.01.001

Dehay, C. and Kennedy, H. (2007). Cell-cycle control and cortical development. *Nat. Rev. Neurosci.* **8**, 438-450. doi:10.1038/nrn2097

Delalle, I., Takahashi, T., Nowakowski, R. S., Tsai, L. H. and Caviness, V. S. (1999). Cyclin E-p27 opposition and regulation of the G1 phase of the cell cycle in the murine neocortical PVE: a quantitative analysis of mRNA in situ hybridization. *Cereb. Cortex* **9**, 824-832. doi:10.1093/cercor/9.8.824

Durak, O., Gao, F., Kaeser-Woo, Y. J., Rueda, R., Martorell, A. J., Nott, A., Liu, C. Y., Watson, L. A. and Tsai, L. H. (2016). Chd8 mediates cortical neurogenesis via transcriptional regulation of cell cycle and Wnt signaling. *Nat. Neurosci.* **19**, 1477-1488. doi:10.1038/nn.4400

Fidler, D. J., Bailey, J. N. and Smalley, S. L. (2000). Macrocephaly in autism and other pervasive developmental disorders. *Dev. Med. Child Neurol.* **42**, 737-740. doi:10.1017/S0012162200001365

Fombonne, E., Rogé, B., Claverie, J., Courty, S. and Frémolle, J. (1999). Microcephaly and macrocephaly in autism. *J. Autism Dev. Disord.* **29**, 113-119. doi:10.1023/A:1023036509476

Gerrard, L., Rodgers, L. and Cui, W. (2005). Differentiation of human embryonic stem cells to neural lineages in adherent culture by blocking bone morphogenetic protein signaling. *Stem Cells* **23**, 1234-1241. doi:10.1634/stemcells.2005-0110

Gervais, L., van den Beek, M., Josserand, M., Sallé, J., Stefanutti, M., Perdigoto, C. N., Skorski, P., Mazouni, K., Marshall, O. J., Brand, A. H. et al. (2019). Stem cell proliferation is kept in check by the chromatin regulators kismet/chd7/chd8 and trr/mll3/4. *Dev. Cell* **49**, 556-573.e6. doi:10.1016/j.devcel.2019.04.033

Gompers, A. L., Su-Feher, L., Ellegood, J., Copping, N. A., Riyadh, M. A., Stradleigh, T. W., Pride, M. C., Schaffler, M. D., Wade, A. A., Catta-Preta, R. et al. (2017). Germline Chd8 haploinsufficiency alters brain development in mouse. *Nat. Neurosci.* **20**, 1062-1073. doi:10.1038/nn.4592

Helsmoortel, C., Vulto-van Silfhout, A. T., Coe, B. P., Vandeweyer, G., Rooms, L., van den Ende, J., Schuurs-Hoeijmakers, J. H., Marcelis, C. L., Willemsen, M. H., Vissers, L. E. et al. (2014). A SWI/SNF-related autism syndrome caused by de novo mutations in ADNP. *Nat. Genet.* **46**, 380-384. doi:10.1038/ng.2899

Hota, S. K. and Bruneau, B. G. (2016). ATP-dependent chromatin remodeling during mammalian development. *Development* **143**, 2882-2897. doi:10.1242/dev.128892

Jung, H., Park, H., Choi, Y., Kang, H., Lee, E., Kweon, H., Ellegood, J., Rhim, I., Bae, M., Kim, S.-G. et al. (2018). Sexually dimorphic behavior, neuronal activity, and gene expression in Chd8-mutant mice. *Nat. Neurosci.* **21**, 1218-1228. doi:10.1038/s41593-018-0208-z

Katayama, Y., Nishiyama, M., Shoji, H., Ohkawa, Y., Kawamura, A., Sato, T., Takumi, T., Miyakawa, T. and Nakayama, K. I. (2016). CHD8 haploinsufficiency results in autistic-like phenotypes in mice. *Nature* **537**, 675-679. doi:10.1038/nature19357

Kobayashi, T., Hashimoto, K., Okumura, H., Asada, H. and Yoshikawa, K. (1998). Endogenous EGF-family growth factors are necessary for the progression from the G1 to S phase in human keratinocytes. *J. Invest. Dermatol.* **111**, 616-620. doi:10.1046/j.1523-1747.1998.00331.x

Lai, W. K. M. and Pugh, B. F. (2017). Understanding nucleosome dynamics and their links to gene expression and DNA replication. *Nat. Rev. Mol. Cell Biol.* **18**, 548-562. doi:10.1038/nrm.2017.47

Lange, C., Huttner, W. B. and Calegari, F. (2009). Cdk4/cyclinD1 overexpression in neural stem cells shortens G1, delays neurogenesis, and promotes the generation and expansion of basal progenitors. *Cell Stem Cell* **5**, 320-331. doi:10.1016/j.stem.2009.05.026

Liu, X., Yan, S., Zhou, T., Terada, Y. and Erikson, R. L. (2004). The MAP kinase pathway is required for entry into mitosis and cell survival. *Oncogene* **23**, 763-776. doi:10.1038/sj.onc.1207188

Liu, W., Dong, W., Hoffman, E. J., Fernandez, T. V. and Gupta, A. R. (2019). *CHD8* regulates the balance between proliferation and differentiation of human iPSCs in neural development. *BioRxiv*. doi:10.1101/732693

Lukaszewicz, A., Savatier, P., Cortay, V., Kennedy, H. and Dehay, C. (2002). Contrasting effects of basic fibroblast growth factor and neurotrophin 3 on cell cycle kinetics of mouse cortical stem cells. *J. Neurosci.* **22**, 6610-6622. doi:10.1523/JNEUROSCI.22-15-06610.2002

Lukaszewicz, A., Savatier, P., Cortay, V., Giroud, P., Huissoud, C., Berland, M. and Dehay, C. (2005). G1 phase regulation, area-specific cell cycle control, and cytoarchitectonics in the primate cortex. *Neuron* **47**, 353-364. doi:10.1016/j.neuron.2005.06.032

Menon, T., Yates, J. A. and Bochar, D. A. (2010). Regulation of androgen-responsive transcription by the chromatin remodeling factor CHD8. *Mol. Endocrinol.* **24**, 1165-1174. doi:10.1210/me.2009-0421

Mohapatra, B., Ahmad, G., Nadeau, S., Zutshi, N., An, W., Scheffe, S., Feng, D., Goetz, B., Arya, P., Bailey, T. A. et al. (2013). Protein tyrosine kinase regulation by ubiquitination: critical roles of Cbl-family ubiquitin ligases. *Biochim. Biophys. Acta* **1833**, 122-139. doi:10.1016/j.bbamcr.2012.10.010

Muratore, C. R., Srikanth, P., Callahan, D. G. and Young-Pearse, T. L. (2014). Comparison and optimization of hiPSC forebrain cortical differentiation protocols. *PLoS One* **9**, e105807. doi:10.1371/journal.pone.0105807

Neganova, I., Zhang, X., Atkinson, S. and Lako, M. (2009). Expression and functional analysis of G1 to S regulatory components reveals an important role for CDK2 in cell cycle regulation in human embryonic stem cells. *Oncogene* **28**, 20-30. doi:10.1038/onc.2008.358

Neganova, I., Vilella, F., Atkinson, S. P., Lloret, M., Passos, J. F., von Zglinicki, T., Burks, D., Jones, R., Armstrong, L. and Lako, M. (2011). An important role for CDK2 in G1 to S checkpoint activation and DNA damage response in human embryonic stem cells. *Stem Cells* **29**, 651-659. doi:10.1002/stem.620

Nowakowski, R. S., Lewin, S. B. and Miller, M. W. (1989). Bromodeoxyuridine immunohistochemical determination of the lengths of the cell cycle and the DNA-synthetic phase for an anatomically defined population. *J. Neurocytol.* **18**, 311-318. doi:10.1007/BF01190834

O'Roak, B. J., Vives, L., Fu, W., Egertson, J. D., Stanaway, I. B., Phelps, I. G., Kumar, A., Lee, C., Ankenman, K., Munson, J. et al. (2012). Multiplex targeted sequencing identifies recurrently mutated genes in autism spectrum disorders. *Science* **338**, 1619-1622. doi:10.1126/science.1227764

Pajalunga, D., Mazzola, A., Franchitto, A., Puggioni, E. and Crescenzi, M. (2008). Molecular and cellular basis of regeneration and tissue repair: the logic and regulation of cell cycle exit and reentry. *Cell. Mol. Life Sci.* **65**, 8-15. doi:10.1007/s00018-007-7425-z

Pauklin, S. and Vallier, L. (2013). The cell-cycle state of stem cells determines cell fate propensity. *Cell* **155**, 135-147. doi:10.1016/j.cell.2013.08.031

Platt, R. J., Zhou, Y., Slaymaker, I. M., Shetty, A. S., Weisbach, N. R., Kim, J.-A., Desai, M., Sood, S., Kempton, H. R., Crabtree, G. R. et al. (2017). Chd8 mutation leads to autistic-like behaviors and impaired striatal circuits. *Cell Rep.* **19**, 335-350. doi:10.1016/j.celrep.2017.03.052

Ran, F. A., Hsu, P. D., Wright, J., Agarwala, V., Scott, D. A. and Zhang, F. (2013). Genome engineering using the CRISPR-Cas9 system. *Nat. Protoc.* **8**, 2281-2308. doi:10.1038/nprot.2013.143

Rodríguez-Paredes, M., Ceballos-Chávez, M., Esteller, M., García-Domínguez, M. and Reyes, J. C. (2009). The chromatin remodeling factor CHD8 interacts with elongating RNA polymerase II and controls expression of the cyclin E2 gene. *Nucleic Acids Res.* **37**, 2449-2460. doi:10.1093/nar/gkp101

Sakaue-Sawano, A., Kurokawa, H., Morimura, T., Hanyu, A., Hama, H., Osawa, H., Fukami, K., Miyata, T., Miyoshi, H., Imamura, T. et al. (2008). Visualizing spatiotemporal dynamics of multicellular cell-cycle progression. *Cell* **132**, 487-498. doi:10.1016/j.cell.2007.12.033

Sawada, G., Ueo, H., Matsumura, T., Uchi, R., Ishibashi, M., Mima, K., Takahashi, Y., Akiyoshi, S., Sudo, T., Sugimachi, K. et al. (2013). CHD8 is an independent prognostic indicator that regulates Wnt/β-catenin signaling and the cell cycle in gastric cancer. *Oncol. Rep.* **30**, 1137-1142. doi:10.3892/or.2013.2597

Shingleton, J. R. and Hemann, M. T. (2015). The chromatin regulator CHD8 is a context-dependent mediator of cell survival in murine hematopoietic malignancies. *PLoS One* **10**, e0143275. doi:10.1371/journal.pone.0143275

Subtil-Rodríguez, A., Vázquez-Chávez, E., Ceballos-Chávez, M., Rodríguez-Paredes, M., Martín-Subero, J. I., Esteller, M. and Reyes, J. C. (2014). The chromatin remodeller CHD8 is required for E2F-dependent transcription activation of S-phase genes. *Nucleic Acids Res.* **42**, 2185-2196. doi:10.1093/nar/gkt1161

Suetterlin, P., Hurley, S., Mohan, C., Riegman, K. L. H., Pagani, M., Caruso, A., Galbusera, A., Crespo-Enriquez, I., Michetti, C., Yee, Y. et al. (2018). Altered neocortical gene expression, brain overgrowth and functional over-connectivity in chd8 haploinsufficient mice. *Cereb. Cortex* **28**, 2192-2206. doi:10.1093/cercor/bhy058

Sugathan, A., Biagioli, M., Golzio, C., Erdin, S., Blumenthal, I., Manavalan, P., Brand, H., Lucente, D., Miles, J., Sheridan, S. D. et al. (2014). CHD8 regulates neurodevelopmental pathways associated with autism spectrum disorder in neural progenitors. *Proc. Natl. Acad. Sci. U.S.A.* **111**, E4468-E4477. doi:10.1073/pnas.1405266111

Varga, E. A., Pastore, M., Prior, T., Herman, G. E. and McBride, K. L. (2009). The prevalence of PTEN mutations in a clinical pediatric cohort with autism spectrum disorders, developmental delay, and macrocephaly. *Genet. Med.* **11**, 111-117. doi:10.1097/GIM.0b013e31818fd762

Wang, P., Mokhtari, R., Pedrosa, E., Kirschenbaum, M., Bayrak, C., Zheng, D. and Lachman, H. M. (2017). CRISPR/Cas9-mediated heterozygous knockout of the autism gene CHD8 and characterization of its transcriptional networks in cerebral organoids derived from iPS cells. *Mol Autism* **8**, 11. doi:10.1186/s13229-017-0124-1

Watanabe, N., Kageyama, R. and Ohtsuka, T. (2015). Hbp1 regulates the timing of neuronal differentiation during cortical development by controlling cell cycle progression. *Development* **142**, 2278-2290. doi:10.1242/dev.120477

Weiss, K., Terhal, P. A., Cohen, L., Bruccoleri, M., Irving, M., Martinez, A. F., Machol, K., Yang, Y., Liu, P., Walkiewicz, M. et al. (2016). De novo mutations in CHD4, an ATP-dependent chromatin remodeler gene, cause an intellectual disability syndrome with distinctive dysmorphisms. *Am. J. Hum. Genet.* **99**, 934-941. doi:10.1016/j.ajhg.2016.08.001

Ziv, O., Zaritsky, A., Yaffe, Y., Mutukula, N., Edri, R. and Elkabetz, Y. (2015). Quantitative live imaging of human embryonic stem cell derived neural rosettes reveals structure-function dynamics coupled to cortical development. *PLoS Comput. Biol.* **11**, e1004453. doi:10.1371/journal.pcbi.1004453